Biosensors and Bioelectronics 55 (2014) 464–469

Contents lists available at ScienceDirect

Biosensors and Bioelectronics

journal homepage: www.elsevier.com/locate/bios

Multi-nanomaterial electrochemical biosensor based on label-free graphene for detecting cancer biomarkers

Bing Jin [a,b], Ping Wang [a,b], Hongju Mao [a,*], Bing Hu [c], Honglian Zhang [a], Zule Cheng [a,b], Zhenhua Wu [a,b], Xiaojun Bian [a], Chunping Jia [a], Fengxiang Jing [a], Qinghui Jin [a], Jianlong Zhao [a]

[a] State Key Laboratory of Transducer Technology, Shanghai Institute of Microsystem and Information Technology, Chinese Academy of Science, Shanghai 200050, China
[b] University of Chinese Academy of Sciences, No. 19A Yuquan Road, Beijing 100049, China
[c] Clinical Research Center of Biological Sensing Technology, Shanghai Xuhui Central Hospital, Shanghai 200040, China

ARTICLE INFO

Article history:
Received 30 September 2013
Received in revised form
3 December 2013
Accepted 10 December 2013
Available online 19 December 2013

Keywords:
Electrochemical biosensor
Graphene
Gold nanoparticle
Magnetic bead
Cancer markers

ABSTRACT

Developing a rapid, accurate and sensitive electrochemical biosensor for detecting cancer biomarkers is important for early detection and diagnosis. This work reports an electrochemical biosensor based on a graphene (GR) platform which is made by CVD, combined with magnetic beads (MBs) and enzyme-labeled antibody-gold nanoparticle bioconjugate. MBs coated with capture antibodies (Ab1) were attached to GR sheets by an external magnetic field, to avoid reducing the conductivity of graphene. Sensitivity was also enhanced by modifying the gold nanoparticles (AuNPs) with horseradish peroxidase (HRP) and the detection antibody (Ab2), to form the conjugate Ab2–AuNPs–HRP. Electron transport between the electrode and analyte target was accelerated by the multi-nanomaterial, and the limit of detection (LOD) for carcinoembryonic antigen (CEA) reached 5 ng mL^{-1}. The multi-nanomaterial electrode GR/MBs–Ab1/CEA/Ab2–AuNPs–HRP can be used to detect biomolecules such as CEA. The EC biosensor is sensitive and specific, and has potential in the detection of disease markers.

1. Introduction

A biomarker is a characteristic that is objectively measured and evaluated, as an indicator of normal biological processes, pathogenic processes, or pharmacological responses to therapeutic intervention (Atkinson et al., 2001). Evaluating serum protein biomarker levels complements methods of detecting and staging tumors, tracking tumor recurrence or metastasis, determining responses to therapies, and estimating the prognosis of such patients. Developing highly sensitive biosensors to detect biomolecules such as cancer protein biomarkers (Chikkaveeraiah et al., 2012) has potential in the early detection of cancer.

Various strategies have been developed for detecting cancer biomarker proteins, including enzyme-linked immunosorbent assay (ELISA) (Voller et al., 1978), radioimmunoassay (RIA) (Goldsmith and Stanley, 1975), electrophoretic immunoassay (Schmalzing and Nashabeh, 1997) and mass spectrometry-based proteomics (Aebersold and Mann, 2003). These techniques often involve sophisticated instrumentation, significant sample volumes, limited sensitivity, and clinically unrealistic expense and measurement times. A simple, rapid, sensitive and economical method for protein measurement at point-of-care and in research applications is required.

Electrochemical (EC) sensors exhibit high sensitivity and specificity, and involve relatively simple instrumentation. They can potentially be expanded into multiplex detection platforms (Liao et al., 2006; Mani et al., 2009; Wei et al., 2008). Voltammetry (linear sweep, differential pulse, square-wave and stripping) and amperometry are the most widely used EC detection methods. They involve a tracer antibody labeled with an electroactive species, such as an enzyme, metal nanoparticle or quantum dot. The tracer is allowed to bind with an analyte, possibly through an intermediate primary antibody, and is thus immobilized on an electrode surface. The concentration of the targeted biomarker is quantified by applying a potential, and measuring the resulting current at the electrode. A variety of immunosensors for detecting cancer biomarkers are available.

The recent development of nanotechnology has advanced EC sensor detections. Nanomaterials can be used in various aspects of the detection system, including in capture probes, reporting molecules and electrode fabrication and coatings (Lord and Kelley, 2009; Ozsoz et al., 2003; Pandey et al., 2008; Radwan and Azzazy, 2009;

* Corresponding author. Tel.: +86 21 62511070 8707; fax: +86 21 62511070 8714.
E-mail address: hjmao@mail.sim.ac.cn (H. Mao).

0956-5663/$ - see front matter Crown Copyright © 2013 Published by Elsevier B.V. All rights reserved.
http://dx.doi.org/10.1016/j.bios.2013.12.025

Zhu et al., 2012). Much attention has been focused on signal amplification using nanomaterial as carriers in EC sensors.

Graphene (GR) is an excellent nanomaterial for EC applications, with its two-dimensional sheets of sp^2-hybridized C atoms in chexagonal configuration (Pumera et al., 2010). The properties of GR include fast electron transportation, high thermal conductivity, excellent mechanical stiffness and good biocompatibility (Li et al., 2008), which result in its promising application in nanocomposites (Stankovich et al. 2006), field-effect transistors (Lee. et al., 2012; Lin. et al., 2013), electromechanical resonators (Bunch et al., 2007) and solar cells (Hsu et al., 2012). The reduced graphene nanowalls (RGNWs) were efficient in label-free detection of single nucleotide polymorphisms of 20 zM oligonucleotides (~10 DNA/mL) with a specific sequence and could effectively contribute to the development of ultra-high-sensitive electrochemical biosensors with single-DNA solution (Akhavan et al., 2012).

Gold nanoparticle-based probes exhibit high sensitivity and stability and low cost, which are advantageous in rapid high-throughput detection methods. Gold nanoparticles (AuNPs) have high surface areas and interesting physicochemical properties. They can be conjugated with DNA, antibodies, enzymes and other biomolecules (Jia et al., 2009). AuNPs are used widely in developing biochemical detection platforms, for detecting various substances including algal cells and toxins (Gas et al., 2010; Zhou et al., 2009), insecticides (Blažková et al., 2009; Wang et al., 2005), metal ions (Tang et al., 2010; Zhou et al., 2010) and proteins (Dykman et al., 2005; Harrison et al., 2008; Sánchez-Martínez et al., 2009). Nanoscale structures of magnetic beads (MBs) have fast reaction kinetics compared with bulk solid surfaces, high surface area per unit volume (owing to their small diameter) and good stability. The relative ease of MBs′ surface modification with functional groups, DNA, enzymes or antibodies has led to their use in the development of sensitive, rapid EC immunoassay systems (Mani et al., 2011; Xie and Jon, 2012).

An EC sensor based on multi-nanomaterials was designed to be used as a potential alternative to detect the model protein carcinoembryonic antigen (CEA), with rapid response time and recovery time compared with the traditional detection, and also as a model protein detection with high sensitivity, specificity and stability. Patients with elevated pretreatment serum levels of CEA (Suzuki et al., 1999; Muley et al., 2003; Kulpa et al., 2002; Nisman et al., 1999; Sawabata et al., 2002) have shorter survival times than those with normal marker concentrations (CEA < 10 ng mL^{-1}). GR, MBs and AuNPs were used to amplify the detection signal. MBs coated with capture antibodies (Ab1) were attracted to isolated GR sheets by an external magnetic field, to give MBs–Ab1. This avoided reducing the conductivity of GR. Sensitivity was also enhanced by modifying the gold nanoparticles (AuNPs) with horseradish peroxidase (HRP) and the detection antibody (Ab2). This resulted in a CEA detection limit of 5 ng mL^{-1}, meeting the requirements for clinical diagnosis (Molina et al., 2003).

2. Materials and methods

2.1. Chemicals and materials

HRP, BSA, 1-(3-(dimethylamino)-propyl)-3-ethylcarbodiimide-hydrochloride (EDC) and N-hydroxysulfosuccinimide (NHS) were obtained from Sigma-Aldrich (CA, USA), and ammonium persulfate ($(NH_4)S_2O_8$) and acetone from Ling Feng Chemical Reagent Co. Ltd. (Shanghai, PR China). Potassium hexacyanoferrate were obtained from Sinopharm Group Co. Ltd. (Beijing, PR China). Carboxylic magnetic beads (diameter ~1 um, composed of highly cross-linked with magnetic material precipitated in pores evenly distributed throughout the beads and further coated with a carboxyl layer of that seals the iron inside the beads) were purchased from Invitrogen (CA, USA). CEA was purchased from Medix Biochemica (Finland). 0.01 M phosphate-buffered saline (PBS, pH 7.4) and 50 mM 2-(N-morpholino) ethanesulfonic acid (MES, pH 6.0) were used as the incubating and washing buffers.

2.2. Preparation of graphene electrode

Graphene films were primarily grown on 25 μm thick Cu through chemical vapor deposition (CVD). The growth process is as follow: (1) the fused silica tube was loaded with the Cu soil, evacuated, backed fill with hydrogen, heated to 1000 °C and maintained a H_2 pressure of 40 mTorr under a 2 sccm flow; (2) the Cu film was stabilized at the desired temperatures, up to 1000 °C,and introduced 35 sccm of CH_4 for a desired period of time at a total pressure of 500 mTorr; and (3) after exposure to CH_4, the furnace was cooled to room temperature. Then the copper substrate was dissolved by $(NH_4)S_2O_8$ solution within 4 h. The concentration of $(NH_4)S_2O_8$ solution is 30–50 g/L. The graphene was rinsed for 5 times with ultrapure water after etching. In this process glass sheet was used to refloat the graphene thin layer. The cleaned graphene was fixed on the $Si+SiO_2$ substrate, then put in the drying oven at 80 °C for 30 min. The substrate with graphene was dipped in acetone for 12 h to remove the organic polymer material PDDA. Finally, the graphene was treated by thermal annealing after removing the PDDA.

2.3. Preparation of Ab2–AuNPs–HRP

20 nm diameter colloidal AuNP solutions were prepared as described by (Zhou et al. 2012). Ab2–AuNPs–HRP was prepared as follows. A 200 μL solution of colloidal AuNPs was adjusted to pH 6.8 using 2 μL of K_2CO_3 solution (0.1 wt%). A 2 mL aqueous solution containing 80 μM EDC and 80 μM NHS was added, to activate the surface of the nanoparticles. Ab2 (1 μL, 1 mg mL^{-1}) and HRP (1 μL, 1 mg mL^{-1}) were added. Biomolecules were electrostatically adsorbed to negatively charged nanoparticle surfaces. After 10 min, the solution was centrifuged at 4 °C and 9000 rpm for 50 min. The supernatant was discarded, and the solids resuspended in 100 μL of PBS containing BSA (0.1 wt%).Ab2–AuNPs–HRP was stored at 4 °C until use.

2.4. Preparation of MBs–Ab1

MBs (50 μL, 10 mg mL^{-1}) were washed for 10 min with MES (50 μL, pH 6.0) twice. The vessel containing the solution was placed on a magnet, and the resulting supernatant discarded. An aqueous solution of EDC (50 μL, 50 mg mL^{-1}) and NHS (50 μL, 5 mg mL^{-1}) in MES was added to the washed MBs, and the resulting solution incubated in a hybridization instrument for 30 min at 25 °C and 4 rpm. The supernatant was again discarded under magnetization conditions. Activated MBs were washed with PBS twice, and the supernatant was removed by magnetization. 1 mg of MBs were added to 50 μg of Ab1 (1 μg mL^{-1}), and incubated in the hybridization instrument for 1 h at 25 °C and 4 rpm. Modified MBs were collected by magnetization, and tris–HCl (150 μL, 50 mM) in PBS was added to deactivate any unbound carboxyl groups. The coated MBs were washed with BSA (0.1 wt%) and Tween20 (0.1 wt%) in PBS, and the final MBs–Ab1 solution was stored at 4 °C until use.

2.5. Preparation of the multi-nanomaterial electrode

10 μL of target antigen was added to the MBs–Ab1 solution, and the resulting solution incubated at room temperature for 15 min. After discarding the supernatant by magnetization, 20 μL

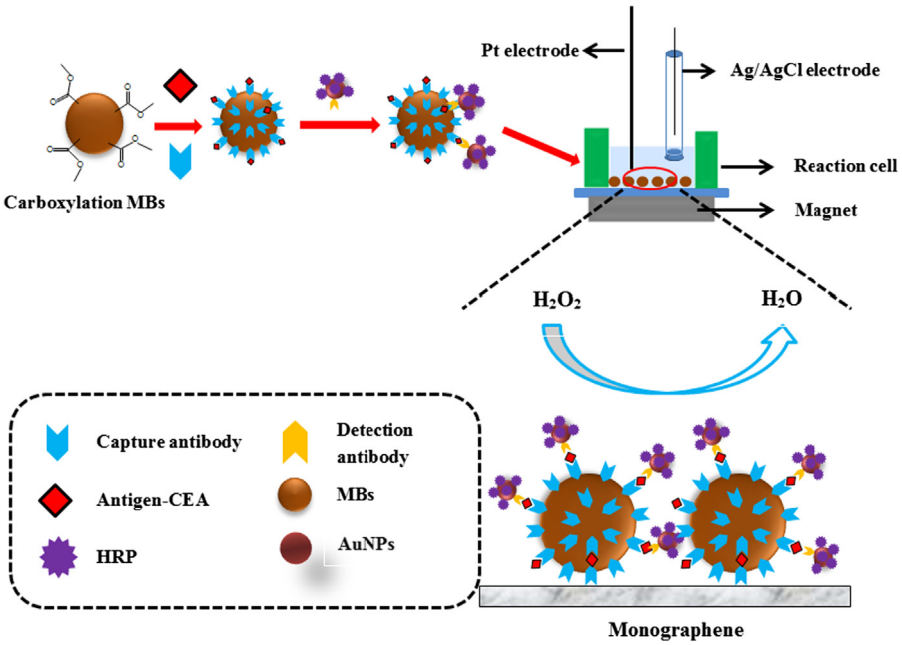

Fig. 1. Preparation of the multi-nanomaterial EC biosensor, and CEA detection procedure.

of Ab2–AuNPs–HRP solution was added, and the resulting solution was incubated at room temperature for 20 min. 10 μL of the resulting immunosystem solution was added dropwise to the GR electrode, which was placed on a magnet. The electrode was gently washed with PBS. The biosensor fabrication process is illustrated in Fig. 1.

3. Results and discussion

3.1. Characterization of GR and graphene oxide (GO)

Raman spectra were measured on Si/SiO_2 substrates at room temperature, with a Renishaw spectrometer at 514 and 633 nm, with 100 cm^{-1} notch filters (Novoselov et al. 2004). Fig. S1 shows the Raman spectra of GR, which possess ordered and disordered crystal structures, respectively. The G bands of GR occurred at G^{GR} ~1580 cm^{-1}, because of the doubly degenerate zone centered E_{2g} mode. The single intense 2D peak at 2680 cm^{-1} in the spectrum of GR was due to two phonons with opposite momentum in the highest optical branch, and the single layer graphene has sharp and intensive 2D peak which is higher than G peak, however, the multi-layer GR has lower 2D peak than its G peak. Especially, the single-layer GR has far more graeter $I_{(2D)}/I_{(G)}$ than the multi-layer GR. Moreover, X-ray photoelectron spectroscopy (XPS) was shown in Fig.S2, to demonstrate the surface chemical composition of GR. The peak of C 1 s at 285 eV mainly relates to C–C and C=C bonds, and 288.1 eV relate to C=O (Akhavan et al., 2012). It showed that, the GR we fabricated from CVD has a trace of C=O/C–O.

3.2. Characterization of Ab2–AuNPs–HRP and GR/MBs–Ab1/CEA/Ab2–AuNPs

Colloidal AuNPs coated with biomolecules will exhibit a change in their surface plasmon resonance. Particles will aggregate because their size has changed, and their absorption spectra will redshift depending on the dielectric properties of the surrounding matrix or environmental conditions. Altering their surface charge will change their permittivity, and the incident light resonance angle or resonant wavelength will also change. The solution color will also change, and the Ab2–AuNPs–HRP solution appeared light purple. Fig. S3 shows that the absorption spectrum of AuNPs is always dominated by their surface plasmon resonance. Binding Ab2 to the AuNPs caused a redshift in the peak of the colloidal AuNPs at 522–524 nm. The peak shifted to 527 nm in the spectrum of Ab2–AuNPs–HRP.

Fig.S4 shows the FTIR spectra of carboxyl group of magnetic beads (MBs) and MBs–Ab1, MBs–Ab1/CEA/Ab2–AuNPs composite. Broad bands at 3700–3000 cm^{-1} are due to the unevaporated water that high hydrogen-bonded hydroxyl groups ν(H–O). FTIR spectrum recorded for the MBs contains the bands at 2966–2866 cm^{-1} (ν(CH)) and the CEA contains the band at 2203 cm^{-1} (ν(C=C)). Upon carboxyl decoration on the MBs surface the band at 1634 cm^{-1} corresponding to ν(C=O) stretched vibrations of the carboxyl acid. The bands at 1526 and 1344, 1128 cm^{-1} were assigned to ν(NH) and ν(CN) vibrations of amino and peptide bonds (Yuriy et al., 2013). This suggested the interaction between CEA antigen and antibodies (Ab1, Ab2) leads to the formation of the complex composites on the fabricated electrode surface. The SEM image of MBs, MBs–Ab1 and MBs–Ab1/CEA/Ab2–AuNPs were shown in Fig. 2.

3.3. Biosensor characterization

GR acts as a transducer for EC sensing, in the form of high surface area conducting electrode surfaces. Catalytic nanoparticles can be deposited and consequently subjected to EC sensing. Fig. 3 shows the detection of H_2O_2 (0.2 mM, PBS) on different modified GR electrodes (bare GR, PBS on bare GR, GR/MBs–HRP and GR/MBs–Ab1/CEA/Ab2–AuNPs–HRP). According to Fig. 3(a) and (b), it showed that, the bare graphene is not sensitivity enough to H_2O_2. After catalyzing H_2O_2 with HRP, the oxidation peak current dramatically increased upon on the delectrode. This is typical of the catalytic oxidation of Fe(III)-containing HRP. The catalytic mechanism of the reaction of immobilized HRP with H_2O_2 is

$$\text{HRP } (Fe^{3+}) + H_2O_2 \rightarrow \text{Compound I } (Fe^{4+}{=}O) + H_2O \quad (1)$$

$$\text{Compound I } (Fe^{4+}{=}O) + e^- + H^+ \rightarrow \text{Compound II} \quad (2)$$

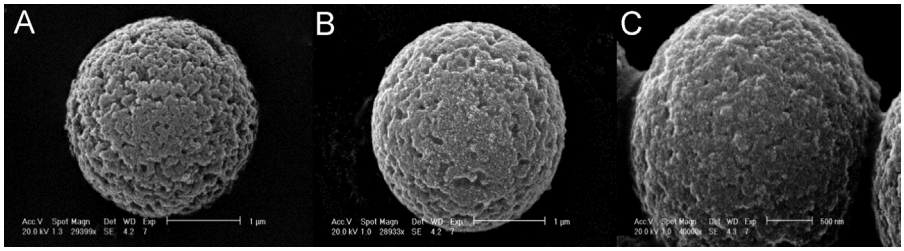

Fig. 2. SEM images of (A) the carboxylic magnetic beads (MBs); (B) MBs–Ab1; and (C) MBs–Ab1/CEA/Ab2–AuNPs.

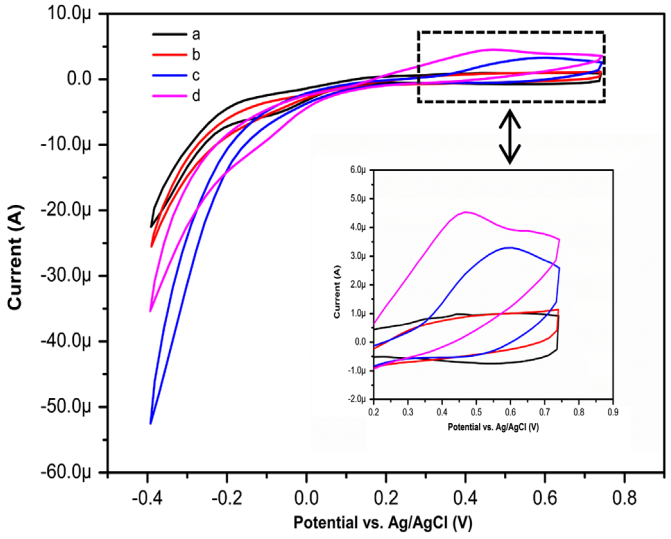

Fig. 3. Detection of H_2O_2 by (a) bare GR, (b) PBS on bare GR (c) GR/MBs–HRP and (d) GR/MBs–Ab1/Ag/Ab2–AuNPs–HRP electrodes. The H_2O_2 concentration was 0.2 mM.

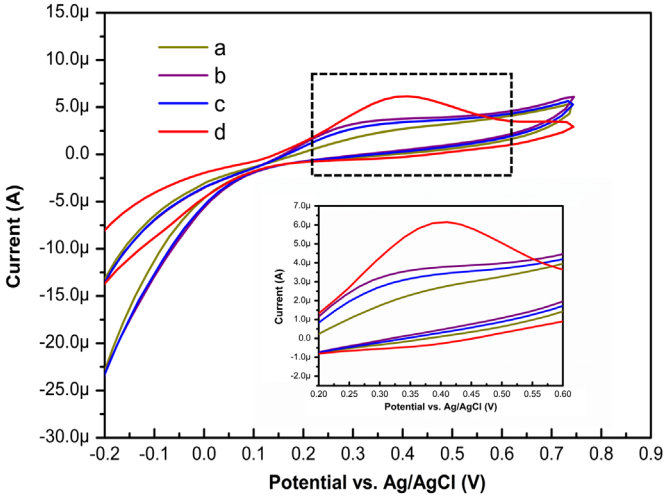

Fig. 4. CV responses of GR/MBs–Ab1 after its immune response with (a) blank, (b) CRP, (c) CY21-1 and (d) CEA. The inset shows an enlargement of the indicated region.

$$\text{Compound II} + e^- + H^+ \rightarrow \text{HRP}(Fe^{3+}) + H_2O \quad (3)$$

For the GR/MBs–Ab1/CEA/Ab2–AuNPs–HRP electrode on the EC work station shown in Fig. S5, the cyclic voltammetry (CV) curve after 20 cycles (~15 min) was stable at −0.4–0.8 V, as the current peak decreased 7.05% (from 6.38 uA to 5.93 uA). From the above catalytic mechanism, oxidation occurs only in the first step, where Fe^{3+} is oxidized to Fe^{4+}. Reduction occurs in each step, so the cathode peak current is much higher than the anode peak.

3.4. Electron transfer dynamics of the GR electrode

The large surface area of the GR electrode is an ideal system for investigating the role of edge planes in EC reactions. The EC behavior associated with the electron transfer (ET) reaction at the GR/solution interface was investigated, using aqueous 0.1 M $K_3Fe(CN)_6$ (Li et al. 2002). ET reactions involving $K_3Fe(CN)_6$ proceed by an inner sphere ET pathway, with the electrode kinetics being sensitive to surface chemistry, microstructure and the density of electronic states near the Fermi potential. Fig. S6(A) shows CV responses to the GR electrode at −0.1–0.8 V, at scan rates of 10–400 mV/s. The EC response indicated a reversible system, with a peak-to-peak potential separation (ΔE_p) of 79–93 mV and a peak current ratio of anode relative to cathode ($R_{a/c}$) of 0.95–1.19. ΔE_p is related to the ET coefficient, and a low ΔE_p indicates fast ET for a single-electron reaction. Fig. S6(B) shows the oxidation and reduction peak currents at scan rates of 10–400 mV/s. The linear relationship indicated single-electron Nernstian behavior, where the EC reaction was controlled by semi-infinite linear diffusion, from the electrolyte to electrode surface.

3.5. Stability and specificity of the multi-nanomaterial electrode

The stability of the multi-nanomaterial electrode was evaluated, as shown in Fig. S3. When detecting CEA, the CV curve exhibited high stability over 20 cycles, compared with the initial response. A small current decrease from 6.38 to 5.93 μA was observed after the electrode was stored for 1 month at room temperature.

The specificity of this biosensor for detecting CEA was investigated, by varying the target antigen including a blank sample (without antigen). C-reactive protein (CRP) and cytokeratin (CY21-1) are potential cancer biomarkers that present at statistically significant levels. Fig. 4 indicates that these cancer biomarker antigens did not immunoconjugate with the CEA detection antibody (Ab2), so would not interfere with the detection of CEA. The high specificity of this biosensor could be attributed to the bioimmune response and the high working electrode surface area.

3.6. Biosensor characterization by electrochemical impedance spectroscopy

Electrochemical impedance spectroscopy (EIS) can be used to characterize EC processes occurring at solution/electrode interfaces. Semicircle portions were observed at high frequencies. This provided information about the capacitance of the solution/electrode interface. It can be deduced by fitting the impedance data using the equivalent circuit. Fig. 5 shows Nyquist plots (Z' vs. Z'') for the different electrodes. EIC measurements were carried out in 0.1 M $K_3Fe(CN)_6$ containing 0.2 M KNO_3. The amplitude was 10 mV and the frequency range was 10 KHz–2 MHz. Bare GR (Fig. 5b) exhibited the smallest semicircle, which was estimated to be 35 Ω.

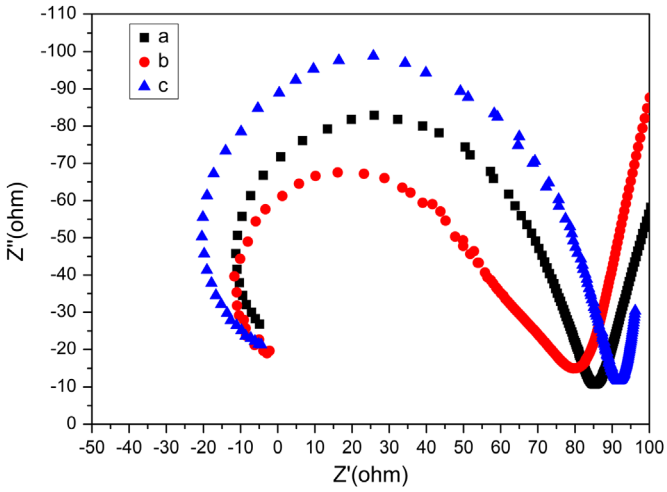

Fig. 5. Nyquist curves of 0.1 M $K_3Fe(CN)_6$ containing 0.2 M KNO_3 for the (a) GR/MBs/AuNPs, (b) bare GR and (c) GR/MBs electrodes. The frequency range was 10 KHz-2 MHz and the amplitude was 10 mV.

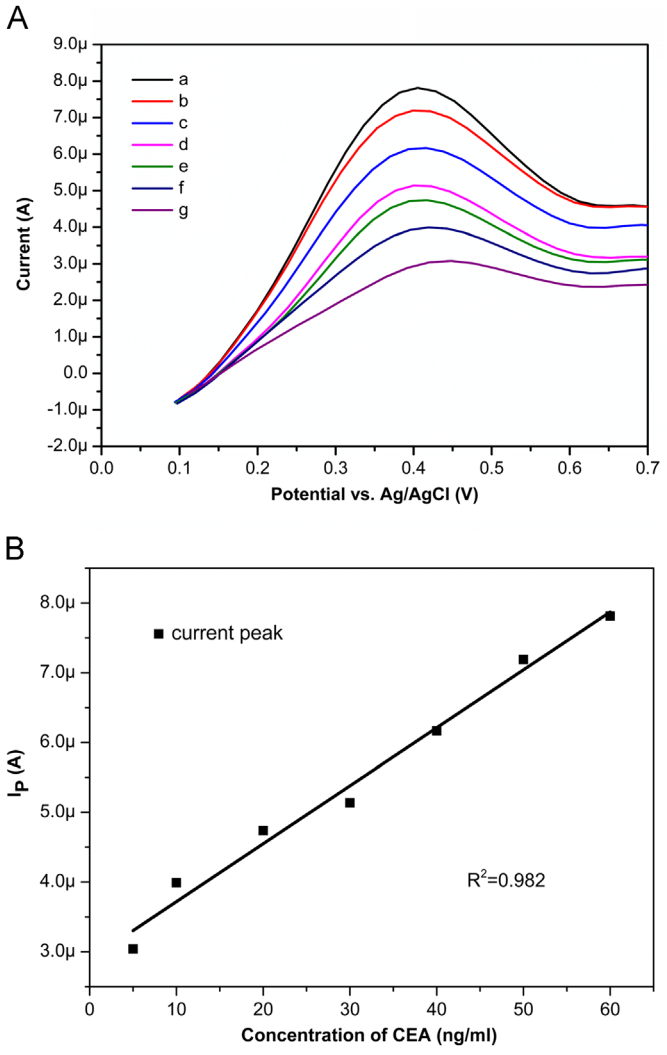

Fig. 6. (A) CV response of GR/MBs–Ab1/CEA/Ab2–AuNPs–HRP for CEA concentrations of (a) 60, (b) 50, (c) 40, (d) 30, (e) 20, (f) 10 and (g) 5 ng mL^{-1}. The scan rate was 100 mV/s. (B) Peak current of CEA vs. concentration (R^2=0.982).

The diameter of the curve in Fig. 5c (105 Ω) was larger than that in Fig. 5a (80 Ω). This suggested that the AuNPs accelerated ET between the electrode and enzyme molecules. The EIS results indicated the immobilization of AuNPs–HRP, and its high electron transfer properties.

3.7. EC response of the immunosensor

The sensitivity and dynamic range of the EC immunosensor were investigated under optimal conditions with CEA, using GR/MBs–Ab1/CEA/Ab2–AuNPs–HRP as a tracer and H_2O_2 as an enzyme substrate, in a sandwich-type immunoassay format. The electrochemical performance of the fabricated electrode was compared to the other modified electrodes for the detection of CEA (Aili et al., 2011; Hongchuan et al., 2011; Hao et al., 2007), which showed the multi-nanomaterial electrochemical biosensor had a high sensitivity and specificity. CV measurements were carried out at pH 7.4 in solution containing 0.2 mM H_2O_2, after incubation with MBs–Ab1 and Ab2–AuNPs–HRP for 15 min at room temperature. Fig. 6A shows that the oxidation peak current of the EC immunosensor increased with increasing CEA concentration. A linear relationship between peak current and CEA concentration was exhibited at 5–60 ng mL^{-1}, $E_{p,a}$ ~0.4 V. The correlation coefficient R was 0.9925 (Fig. 6B). The limit of detection (LOD) was 5 ng mL^{-1}, which meets clinical requirements. The EC immunosensor had a low LOD, and has potential in the early stage diagnosis of cancers.

4. Conclusion

A multi-nanomaterial biosensor based on isolated GR sheets was reported, for the sensitive and specific detection of the cancer-related biomarker CEA. The multi-nanomaterial electrode exhibited a high GR electron transfer rate, and amplified electro-signal by the MBs–AuNPs. The obtained results present a rapid response time and recovery time that are shorter than the traditional strateties. The detection limit was 5 ng mL^{-1}, which meets requirements for clinical diagnosis. The high sensitivity and specificity, ease of fabrication, operational convenience, short analysis time and reusability make this biosensor a promising candidate for the clinical diagnosis of cancer.

Acknowledgments

This work was supported by Grants from the National Basic Research Program of China (973 Program) (Nos. 2012CB933303, 2011CB707505), the National Science Foundation of China (Nos. 21275153, 61006086, 31000791), Science and Technology Commission of Shanghai Municipality (Grant nos. 11nm0505800, 12441902600, 11JC1414400) and Shanghai Institute of Microsystem and Information Technology and Shanghai Clinical Center/ShanghaiXuhui Central Hospital, Chinese Academicof Sciences (No. BRC2012002).

Appendix A. Supplementary material

Supplementary data associated with this article can be found in the online version at http://dx.doi.org/10.1016/j.bios.2013.12.025.

References

Aebersold, R., Mann, M., 2003. Nature 422 (6928), 198–207.
Aili, S., Gairong, C., Qinglin, S., Jianbin, Z., 2011. Biochem. Eng. J. 57, 1–6.
Akhavan, Omid, Ghaderi, Elham, Rahighi, Reza, 2012. Acs Nano 6 (4), 2904–2916.
Atkinson, A.J., Colburn, W.A., DeGruttola, V.G., DeMets, D.L., Downing, G.J., Hoth, D.F., Oates, J.A., Peck, C.C., Schooley, R.T., Spilker, B.A., 2001. Clin. Pharmacol. Ther. 69 (3), 89–95.

Blažková, M., Mičková-Holubová, B., Rauch, P., Fukal, L., 2009. Biosens. Bioelectron. 25 (4), 753–758.
Bunch, J.S., Van Der Zande, A.M., Verbridge, S.S., Frank, I.W., Tanenbaum, D.M., Parpia, J.M., Craighead, H.G., McEuen, P.L., 2007. Science 315 (5811), 490–493.
Chikkaveeraiah, B.V., Bhirde, A.A., Morgan, N.Y., Eden, H.S., Chen, X., 2012. ACS Nano 6 (8), 6546–6561.
Dykman, L.A., Bogatyrev, V.A., Khlebtsov, B.N., Khlebtsov, N.G., 2005. Anal. Biochem. 341 (1), 16–21.
Gas, F., Baus, B., Pinto, L., Compere, C., Tanchou, V., Quéméneur, E., 2010. Biosens. Bioelectron. 25 (5), 1235–1239.
Goldsmith, S.J., Stanley, M.D., 1975. Seminars in Nuclear Medicine 5 (2), 125–152.
Hao, T., Jinhua, C., Lihua, N., Yafei, K., Shouzhuo, Y., 2007. Biosens. Bioelectron. 22, 1061–1067.
Harrison, G., Haffey, P., Golub, E.E., 2008. Anal. Biochem. 380 (1), 1–4.
Hongchuan, Y., Ruo, Y., Yaqin, C., Li, M., Huilan, S., Wen, J., Min, L., 2011. Biochem. Eng. J. 56, 116–124.
Hsu, C.L., Lin, C.T., Huang, J.H., Chu, C.W., Wei, K.H., Li, L.J., 2012. ACS Nano. 6 (6), 5031–5039.
Jia, C.P., Zhong, X.Q., Hua, B., Liu, M.Y., Jing, F.X., Lou, X.H., Yao, S.H., Xiang, J.Q., Jin, Q.-H., Zhao, J.-L., 2009. Biosens. Bioelectron. 24 (9), 2836–2841.
Kulpa, J.,E., Reinfuss, M., Kolodziejski, L., 2002. Clin Chem 48, 1931–1937.
Lee, J., Tao, L., Hao, Y., Ruoff, R.S., Akinwande, D., 2012. Appl. Phys. Lett. 100, 152104.
Li, D., Mueller, M.B., Gilje, S., Kaner, R.B., Wallace, G.G., 2008. Nat. Nanotechnol. 3 (2), 101–105.
Li, J., Cassell, A., Delzeit, L., Han, J., Meyyappan, M., 2002. J. Phys. Chem. B 106 (36), 9299–9305.
Liao, J.C., Mastali, M., Gau, V., Suchard, M.A., Møller, A.K., Bruckner, D.A., Babbitt, J.T., Li, Y., Gornbein, J., Landaw, E.M., 2006. J. Clin. Microbiol. 44 (2), 561–570.
Lin, C.T., Loan, P.T.K., Chen, T.Y., Liu, K.K., Chen, C.H., Wei, K.H., LI, L.J., 2013. Adv. Funct. Master 23 (18), 2301–2307.
Lord, H., Kelley, S.O., 2009. J. Mater. Chem. 19 (20), 3127–3134.
Mani, V., Chikkaveeraiah, B.V., Patel, V., Gutkind, J.S., Rusling, J.F., 2009. ACS Nano 3 (3), 585–594.
Mani, V., Chikkaveeraiah, B.V., Rusling, J.F., 2011. Expert Opin. Med. Diagn. 5 (5), 381–391.
Molina, R., Filella, X., Auge, J.M., Fuentes, R., Bover, I., Rifa, J., Moreno, V., Canals, E., Vinolas, N., Marquez, A., Barreiro, E., Borras, J., Viladiu, P., 2003. Tumor Biol. 24, 209–218.
Muley, T., Dienemann, H., Ebert, W., 2003. Anticancer Res. 23, 4085–4094.
Nisman, B., Amir, G., Lafair, J., Heching, N., Lyass, O., Peretz, T., 1999. Anticancer Res. 19, 3549–3552.
Novoselov, K.S., Geim, A.K., Morozov, S., Jiang, D., Zhang, Y., Dubonos, S., Grigorieva, I., Firsov, A., 2004. Science 306 (5696), 666–669.
Ozsoz, M., Erdem, A., Kerman, K., Ozkan, D., Tugrul, B., Topcuoglu, N., Ekren, H., Taylan, M., 2003. Anal. Chem. 75 (9), 2181–2187.
Pandey, P., Datta, M., Malhotra, B., 2008. Anal. Lett. 41 (2), 159–209.
Pumera, M., Ambrosi, A., Bonanni, A., Chng, E.L.K., Poh, H.L., 2010. TrAC Trends Anal Chem 29 (9), 954–965.
Radwan, S.H., Azzazy, H.M., 2009. Expert Rev. Mol. Diagn. 9 (5), 511–524.
Sánchez-Martínez, M., Aguilar-Caballos, M., Gómez-Hens, A., 2009. Anal. Chim. Acta 636 (1), 58–62.
Sawabata, N., Otha, M., Takeda, SI., Hirano, H., Okumura, Y., Asada, H., 2002. Ann. Thorac. Surg. 74, 174–179.
Schmalzing, D., Nashabeh, W., 1997. Electrophoresis 18 (12-13), 2184–2193.
Stankovich, S., Dikin, D.A., Dommett, G.H., Kohlhaas, K.M., Zimney, E.J., Stach, E.A., Piner, R.D., Nguyen, S.T., Ruoff, R.S., 2006. Nature 442 (7100), 282–286.
Suzuki, K., Nagai, K., Yoshida, J., Moriyama, E., Nishimura, M., Takahashi, K., 1999. Ann. Thorac. Surg. 67, 927–932.
Tang, Y., Zhai, Y.-F., Xiang, J.-J., Wang, H., Liu, B., Guo, C.-W., 2010. Environ. Pollut. 158 (6), 2074–2077.
Voller, A., Bartlett, A., Bidwell, D., 1978. J. Clin. Pathol. 31 (6), 507–520.
Wang, S., Zhang, C., Wang, J., Zhang, Y., 2005. Anal. Chim. Acta 546 (2), 161–166.
Wei, F., Wang, J., Liao, W., Zimmermann, B.G., Wong, D.T., Ho, C.-M., 2008. Nucleic Acids Res. 36 (11), e65.
Xie, J., Jon, S., 2012. Theranostics 2 (1), 122.
Yuriy, A.Chesalov, Galina, B.Chernobay, Tamara, V.Andrushkevich, 2013. J. Mol. Catal. A: Chem. 373, 96–107.
Zhou, Y., Li, Y.-S., Tian, X.-L., Zhang, Y.-Y., Yang, L., Zhang, J.-H., Wang, X.-R., Lu, S.-Y., Ren, H.-L., Liu, Z.-S., 2012. Sens. Actuators B: Chem. 161 (1), 1108–1113.
Zhou, Y., Pan, F.-G., Li, Y.-S., Zhang, Y.-Y., Zhang, J.-H., Lu, S.-Y., Ren, H.-L., Liu, Z.-S., 2009. Biosens. Bioelectron. 24 (8), 2744–2747.
Zhou, Y., Zhang, Y., Pan, F., Li, Y., Lu, S., Ren, H., Shen, Q., Li, Z., Zhang, J., Chen, Q., 2010. Biosens. Bioelectron. 25 (11), 2534–2538.
Zhu, J., Zou, N., Mao, H., Wang, P., Zhu, D., Ji, H., Cong, H., Sun, C., Wang, H., Zhang, F., 2012. Biosens. Bioelectron.